JOURNAL OF MAGNETIC RESONANCE **130,** 272–280 (1998)
ARTICLE NO. MN971300

A Radiofrequency (220-MHz) Fourier Transform EPR Spectrometer

Marcello Alecci, John A. Brivati, Giuseppe Placidi, and Antonello Sotgiu

INFM and Dipartimento di Scienze e Tecnologie Biomediche, Università dell'Aquila, Via Vetoio, 67100 L'Aquila, Italy

Received February 7, 1997; revised July 22, 1997

Radiofrequency continuous wave EPR spectrometers for detecting and localizing free radicals *in vivo* in samples of 50–100 g have been developed. The main limitation of these EPR instruments is the slow acquisition time, and a sensible improvement is expected by the adoption of pulsed EPR techniques. We present here a Fourier transform EPR spectrometer operating at 220 MHz suitable for large volume samples (up to 50 ml). A detailed description of the transmitter and receiver sections, including the EPR resonator, is given. Representative free induction decay data obtained from a sample with a relaxation time of about 900 ns are reported.

Key Words: **EPR; spectrometer; resonator;** *in vivo;* **nitroxide free radicals.**

INTRODUCTION

Radiofrequency (RF) continuous wave (CW) EPR spectrometers for detecting and localizing free radicals *in vivo* have been developed in the past two decades (*1–11*). Many studies have demonstrated that exogenous and endogenous free radicals have a major role in the study of several physiopathological conditions (*12–21*). The main limitation of CW EPR spectroscopy/imaging is the slow acquisition rate. Image reconstruction requires the collection of one-dimensional projections obtained by recording the EPR spectrum in the presence of a magnetic field gradient. As each projection takes about 30–120 s to acquire, and in view of the fact that the field sweep must extend considerably outside the field region containing the sample to permit accurate mathematical treatments, such as deconvolution and reconstruction (*22, 23*), a whole three-dimensional reconstruction requires a total acquisition time of about 30 min and is not compatible with the biological half-life of the usual paramagnetic probes studied. The need for pulsed Fourier transform (FT) EPR techniques is essentially related to this problem, and it is hoped that these techniques will also make possible the observation of transient free radicals that cannot be observed with CW EPR.

In contrast to NMR, the development of FT EPR has been very slow. The main reason is that the most readily available exogenous paramagnetic probes are nitroxide free radicals, in either the protonated or perdeuterated form. Their relaxation times (T_1, T_2) are between 300 ns and 1 μs (*24*), and these give rise to difficulties in the development of an FT EPR apparatus, particularly at low frequencies where the resonator dead time is long. The main instrumental requirements are short receiver dead time, short pulse duration, high pulse power, fast acquisition rate, and fast data transfer to a computer. The first requirement is particularly difficult to meet at low frequencies.

Despite these difficulties, a few homebuilt FT EPR instruments operating in the RF range have been developed, and the first EPR free induction decay (FID) at 17.4 MHz was reported by Blume (*25*), four decades ago, using trapped electrons in liquid ammonia. Sachs *et al.* (*26*) reported a comparison of relaxation times at 192 MHz and 9 GHz using crystals of conducting fluoranthenyl radical cation salt, but no details were given of the EPR instrumentation. More recently, RF FT EPR apparatuses, specifically developed for imaging applications and operating at 300 MHz, have been proposed (*27–28*). These apparatuses adopt a classical duplex configuration that comprises a single TX/RX resonator connected to either the TX or the RX by a duplexer. The duplexer circuit usually necessitates a dummy circuit that acts as an additional load to the transmitter and/or an additional source of noise to the receiver (*29*). Other disadvantages of the previous RF FT EPR apparatuses (*27, 28*) are the very long receiver dead time (T_D) (300 ns to 2 μs) and the very small sample volume (less that 2 ml).

In this paper we describe the overall design of an FT EPR spectrometer operating at 220 MHz. A detailed description of the transmitter (TX) and receiver (RX) sections, including the EPR resonator, is given. We also show that this spectrometer can be adapted for CW detection of EPR spectra. Finally, we report representative FID data obtained from a sample with submicrosecond relaxation times.

FT EPR SPECTROMETER DESIGN

The overall diagram of the RF FT EPR spectrometer is shown in Fig. 1A. It consists of the following main sections: (1) RF source and gating that generates the TX pulse of suitable width and power and the auxiliary pulse for quenching the TX resonator; (2) TX loop–gap resonator (LGR); (3) RX resonator assembly consisting of two pairs of saddle-shaped resonators perpendicular to each other; (4) RF signal

1090-7807/98 $25.00

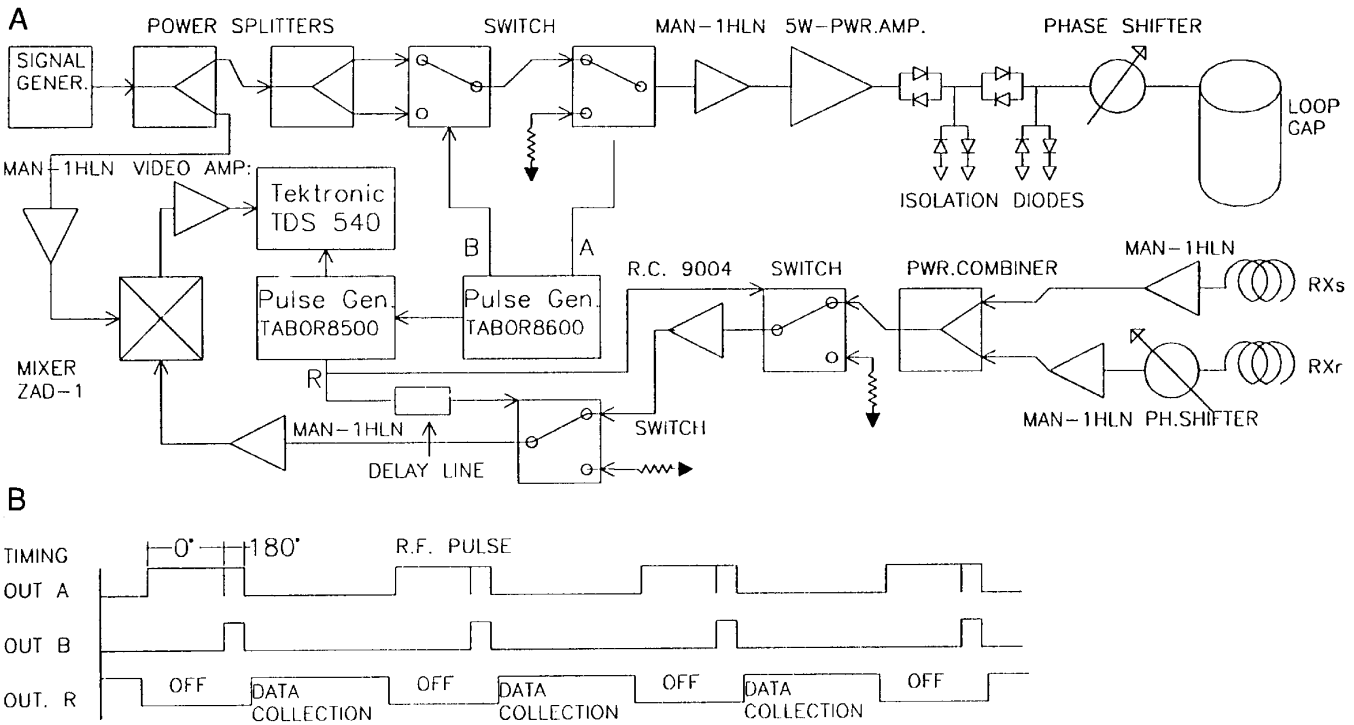

FIG. 1. (A) Overall diagram of the radiofrequency FT EPR spectrometer operating at 220 MHz. (B) Timing diagram for the generation of the TX composite pulse and for the synchronization of the receiver. The electric characteristics of the relevant component are as follows: ZMSC-2-1 (Mini-Circuits, USA), frequency range 0.1–400 MHz, isolation 25 dB min, insertion loss 0.4 dB max, phase unbalance 3° max, amplitude unbalance 0.2 dB max. ZYSW-2-50 DR (Mini-Circuits, USA), insertion loss 1.5 dB max, 1 dB compression point 20 dBm, in/out isolation 50 dB. MAN-1HLN (Mini-Circuits, USA), frequency range 10–500 MHz, noise figure 3 dB max, gain 12 dB, 1 dB compression point 15 dBm. RC 9004 (Research Communications, UK), frequency range 200–240 MHz, noise figure 2 dB max, gain 57 dB, max. output 1 V rsm, settling time 60 ns.

conditioning section where the signals of the two orthogonal channels are combined to reduce the dead time; and (5) analog to digital converter (ADC) and data acquisition/display. In the following we descibe in detail the various sections of the apparatus.

Transmitter Design

The 220-MHz radiofrequency signal required for the transmitter and the local oscillator (LO) reference of the receiver is provided by an HP8640 signal generator. Its output is split by a power divider (Mini-Circuits ZFSCJ-2-1): one output is used to provide the LO, the other is further split by a ZFSCJ-2-1 to provide two 180° out-of-phase signals. These are selected by a two-way switch (Mini-Circuits ZYSWA-2-50DA) controlled by the secondary output of a TABOR 8600 twin pulse generator. The selected output is connected to another switch, controlled by the main pulse of the TABOR 8600 to provide the pulse ON/OFF function. In this way the RF pulse consists of the main RF pulse (200 to 400 ns) plus a phase-reversed auxiliary pulse (30 to 60 ns). The starting time of the auxiliary pulse (and consequently its duration) can be shifted with respect to the main pulse, so as to optimize the dead time reduction of the TX resonator (*30*). The trigger signal (TRIG) from the TABOR 8600 is used to synchronize a second pulse generator (TABOR 8500) that controls the receiver section. The power required to obtain a 90° flip angle depends on the sample loading that modifies the resonator Q factor and, as a consequence, the value of the efficiency factor Λ. For Q values between 170 and 90 and using a pulse length of about 300 ns the required power to obtain a 90° flip angle varies from 1 to 5 W. This power is provided by a Mini-Circuits amplifier (MAN-1HLN) and a class-A power amplifier (Mini-Circuits ZHL-5W-1) that delivers 5-W rms between 1 and 500 MHz. Its output is connected to a back-to-back diode (Philips, BAW62) circuit (*31*) with a $\lambda/4$ line tuned to 220 MHz (Fig. 1). This provides a threshold barrier (minimum 70 dB) to remove the TX pulse falling edge and power amplifier noise during the detection phase. The power amplifier is connected to the TX resonator, via a phase shifter and a standard $\lambda/4$ triaxial balun (*31*), so as to make the cable between the diodes and the TX resonator of length $(2n\text{-}1)\lambda/4$ (Fig. 1). The $\lambda/4$ shunt lines ensure that no transmitter noise reaches the LGR during reception. Combined with the phase shifter it results in a low impedance at the LGR so as to dampen the ringing.

We have also tested a homebuilt class-C power amplifier that delivers 30 W at a central frequency of 220 MHz with

a bandwidth of 30 MHz. The use of the class-C amplifier simplifies considerably the TX design and avoids the use of the diode circuit.

TX and RX Resonators

We used separate TX and RX resonators (crossed-coil configuration) to reduce T_D. The two separate resonators are tuned to the same frequency, and the RF fields are geometrically perpendicular. This gives a high isolation between TX and RX, with a consequent reduction of T_D. A similar design was proposed in the early years of NMR spectroscopy (*32*) and recently in CW NMR imaging of solids (*33*) and in CW and pulsed L-band (1.2 GHz) EPR (*34*). With the crossed-resonator configuration, the choice of the volumes and Q of the TX and RX resonators is a compromise dictated by the maximum TX power available, the dead time, and the sensitivity of the apparatus. As is common practise in pulsed NMR (*29*) and pulsed EPR (*35*), we positioned the TX resonator externally with respect to the RX resonator. This configuration requires the use of higher TX power pulse, but optimizes the filling factor of the RX resonator. At present we are using a TX resonator with high Q because of the limited power provided by the TX power amplifier (max 5 W rms). The availability of an amplifier with higher TX power would make it possible to decrease the Q of the TX resonator, thus reducing the dead time of the pulsed EPR instrument. With the present design the TX resonator has a higher Q with respect to that of the two RX saddle-shaped resonators when empty (TX $Q = 170$ and RX $Q = 100$) or with 55 ml of physiological saline solution (TX $Q = 90$ and RX $Q = 35$). The SNR would benefit from the use of RX resonators with higher Q, but this is not easily achieved with large conductive samples because of the electrical and magnetic losses due to the sample. The TX resonator, see Fig. 2, is a one-loop four-gap resonator (LGR) (*36*) (diameter 59 mm and length 20 mm) made of adhesive copper strip (RS components, UK). The LGR was laid on the internal surface of a Teflon cylinder (external diameter 75 mm, internal diameter 59 mm, length 24 mm) that was inserted into a brass shield (internal diameter 75 mm, length 90 mm). A balanced capacitive network (*31*) was adopted to optimize the LGR tuning/matching. The LGR has an unloaded quality factor Q of about 170 when empty. The efficiency factor $\Lambda = 19\ \mu\mathbf{T}/\sqrt{\mathbf{W}}$ of the empty LGR ($\Lambda = \boldsymbol{B}_1/\sqrt{\boldsymbol{P}}$, where B_1 is amplitude of the RF field and P the incident power) was measured by the perturbing sphere method (*37*). From this value the required peak power to obtain a 90° flip angle with RF pulses of 300 ns was 2.4 W.

The RX resonator, see Fig. 2, is composed of two (identical) pairs of saddle-shaped resonators tuned to 220 MHz, perpendicular to each other and perpendicular to the LGR. In principle, the two receiving resonators (RX_S and RX_R) have identical ringing times. The RX_S resonator (perpendicular to the main magnetic field) is used as the FID receiver, and the RX_R resonator (parallel to the main field) is used to reduce the dead time of the receiver, as reported in detail elsewere (*38*). Each saddle-shaped resonator was made from adhesive copper strip 4 mm wide. The angular aperture of the saddles is 82° and the length is 50 mm. Each saddle-shaped resonator was laid on the external surface of a Teflon cylinder (external diameter 36 mm, internal diameter 30 mm, length 100 mm) that was inserted coaxially into the brass shield. A balanced capacitive network (*31*), positioned outside the brass shield, was adopted to optimize the tuning/matching of each saddle-shaped resonator. The unloaded Q factor of each RX resonator was about 100 when empty.

Receiver Design

The detailed diagram of the receiver is shown in Fig. 1. It differs from standard designs because of the two channels used to reduce the dead time (*38*). The output of the RX_S resonator is preamplified (Mini Circuits, MAN-1-HLN) and connected to the power combiner (Mini Circuits, ZFSCJ-2-1), while the RX_R output is connected to a variable phase shifter (Microlab-FRX Model ST-05), amplified by a low-noise preamplifier (Mini Circuits, MAN-1-HLN), and finally connected to the other input of the power combiner. Because of the finite isolation between the TX and the RX resonators, the same ringing voltages (amplitude and phase) are induced in the RX_S and RX_R resonators. Using the two-channel receiver, when the phases of the two channels were

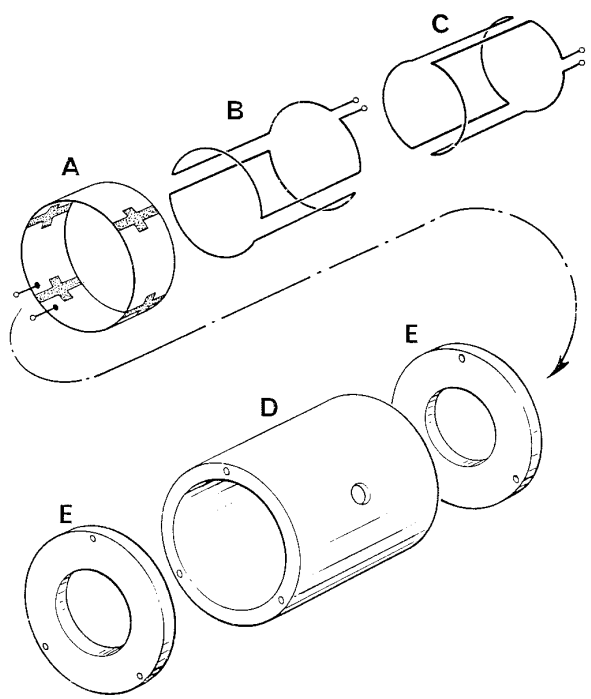

FIG. 2. The resonator assembly for FT EPR detection: (A) TX loop–gap resonator; (B) saddle-shaped RX_S resonator; (C) saddle-shaped RX_R resonator; (D) RF shield; (E) mechanical supports. When in operation the two RX resonators are inserted coaxially within the TX loop–gap resonator.

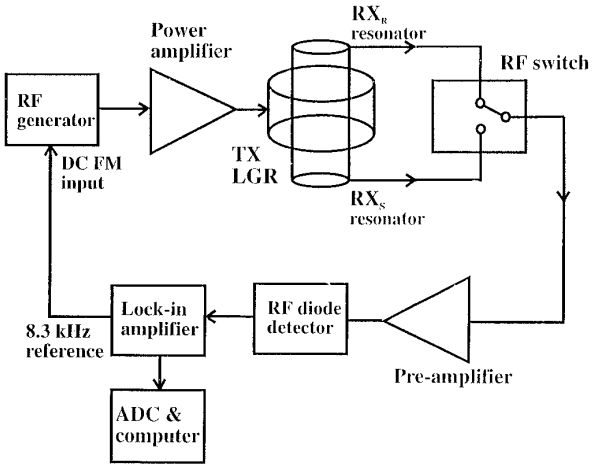

FIG. 3. Schematic design of the radiofrequency EPR spectrometer in CW operation mode at 220 MHz.

exactly out-of-phase we observed a marked reduction of T_D (about 300 ns). For example, if the RX_R is along the stationary field it will not produce any FID and its addition will not disturb the RX_S FID. When RX_R and RX_S have an arbitrary direction with respect to the stationary field, their contribution is always in phase quadrature, the 180° change of phase of one of them will leave them in phase quadrature, and no cancellation of the FID will occur. The power combiner output is connected, via a standard $\lambda/4$ line and crossed-diodes, to an RF switch (Mini-Circuits, ZYSWA-2-50DA) whose function is to further protect the RX during the TX pulse. The switch output is amplified by two cascaded amplifiers (Research Communication Ltd 9004 and Mini-Circuits Man-1HLN) for a total gain of 50 dB. A balanced mixer (Mini-Circuits, ZAD-1) is used for the detection of the FID. The reference signal (+10 dBm) for the local oscillator input of the mixer is obtained after amplification from the main RF source (HP8640B) via a power splitter (Mini-Circuits, ZFSC-2-2). The mixer output, after 20 dB of amplification by a homebuilt video amplifier, is connected to a digital storage oscilloscope (Tektronix, TDS 540) for ADC and data storage/display.

CW EPR Configuration

The FT EPR spectrometer, as described in the previous sections, can be easily adapted for CW EPR measurements, as shown in Fig. 3. This configuration is very useful during tests of the apparatus and for searching for the resonance so as to set the stationary magnetic field. The RF source (HP8640B) output was amplified by a class-A power amplifier (Mini-Circuits ZHL-5W-1) and applied to the TX LGR. The RX_S (or RX_R) coil was used as the receiver channel by connecting its output to a low-noise preamplifier (Mini Circuits, MAN-1-HLN) and detecting the signal with an RF diode. A lock-in amplifier (EG&G 5210) was used for phase-sensitive detection at 8.3 kHz. The thick brass screen of the TX/RX (see Fig. 2) did not allow modulation of the magnetic field at this frequency. For this reason the sinusoidal reference output (8.3 kHz) of the lock-in amplifier was connected to the frequency modulation input of the RF source with a peak deviation of 320 kHz. This configuration is equivalent to the standard use of modulation of the main magnetic field with additional audiofrequency coils, and the recorded spectra are in the first derivative form. The performances of this kind of detection are limited by: (i) the presence of a very high level of modulation offset at the input of the lock-in amplifier that limits the dynamic range of the receiving system; and (ii) the variations of the modulation offset caused by changes in the isolation between the TX and RX resonators. The first limits the dynamic range of the measured signal and the second introduces fluctuations that add to the noise. The use of field modulation is known to give a signal-to-noise ratio (SNR = signal peak height/standard deviation of the noise) better than that of other kinds of modulation (*39*, p. 394), but it cannot be implemented with the current design of the resonator because of the RF shield. No attempt was made to build an automatic frequency control circuit, and the spectra show a mixture of absorption and dispersion components as a result (*40*).

EXPERIMENTAL RESULTS

Isolation and Dead Time Measurement

The isolation between the TX and the RX resonators was measured with 55 ml of physiological saline solution (0.9% weight/volume of NaCl in deionized water) inserted in the resonator. This sample was chosen because it represents a good simulation for *in vivo* experiments (*16*). Under this condition, the quality factor of the TX resonator was about 90 and that of the two RX resonators was about 35. A double-channel network analyzer (Hewlett–Packard, Model HP8753A) and a reflection transmitter kit (Hewlett–Packard, Model HP85044A) were used to measure the reflection coefficient of the LGR and the isolation between TX and RX resonators. The RF output of the network analyzer (acting as the transmitter) was connected via the reflection transmitter kit to the LGR. The reflected power from the LGR was connected via the reflection transmitter kit to the first RF input of the network analyzer for the measurement of the reflection coefficient. The second RF input of the network analyzer was connected to: (i) the RX_S resonator only (or equivalently to the RX_R resonator only); (ii) the output of the power combiner with the RX_S and RX_R resonators in the out-of-phase configurations; or (iii) the output of the power combiner with the RX_S and RX_R resonators in the in-phase configurations. Under these conditions the network analyzer provides the simultaneous measurement of the reflection coefficient of the LGR (see Fig. 4a) and the isolation (see Figs. 4b–4e). The reflection coefficient (S_{11}) is defined as

the ratio in decibels between the incident and the reflected power at the input of the LGR. The isolation (I) between the TX and RX resonators is defined as the ratio in decibels between the incident power in the TX LGR and the power at the output of the RX resonator. As expected, with the out-of-phase condition we found a marked increase of the isolation with a typical value of about 45 dB at the resonant frequency within a bandwidth of a few megahertz, see Fig. 4d. Values of isolation up to 55 dB can be obtained with a careful positioning of the TX resonator with respect to the RX resonator and the tuning/matching of the resonators. We observed also that the isolation could be increased up to 80 dB if the TX LGR was sligthly detuned (±2 MHz) with respect to the RX resonator frequency.

To measure T_D of the receiver, a high power (4 W rms)

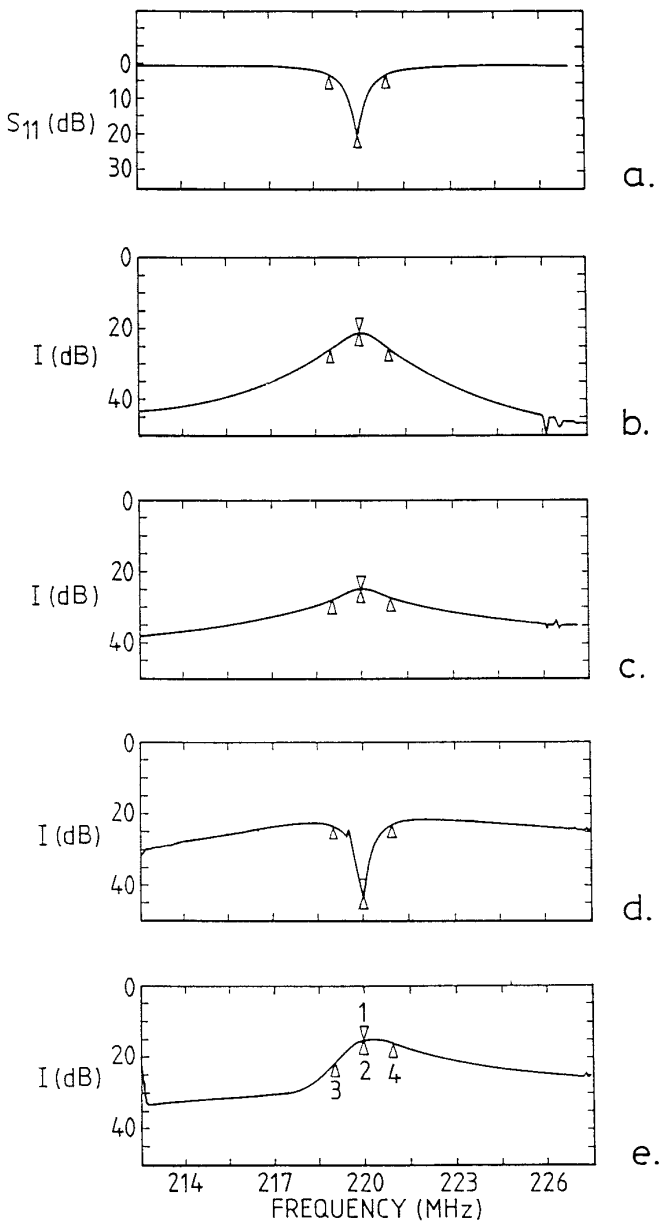

FIG. 4. (a) Measured reflection coefficient of the TX loop–gap resonator. Measured isolation between the TX loop–gap resonator and (b) the RX_R resonator only; (c) the RX_S resonator only; (d) the out-of-phase combination of RX_S and RX_R; and (e) the in-phase combination of RX_S and RX_R.

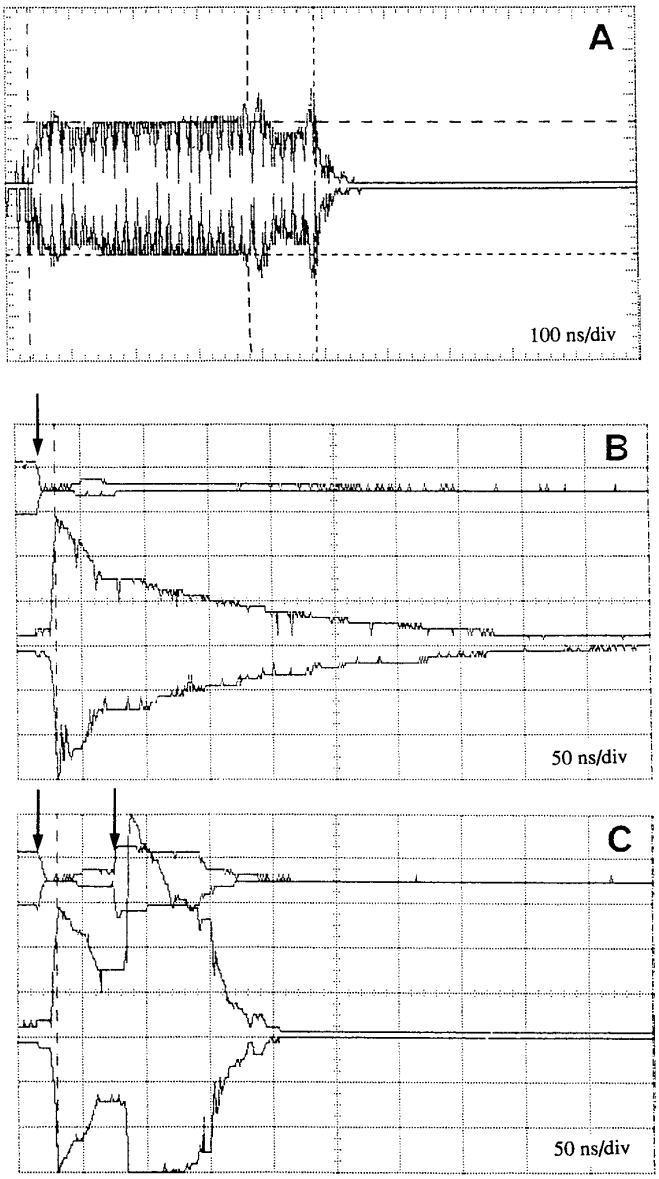

FIG. 5. (A) Typical TX pulse at 220 MHz (5 W rms) composed of the main pulse (width of 350 ns), for the excitation of the electron spin transitions and of the auxiliary pulse (width of 100 ns) for the quenching of the TX resonator. The time scale was 100 ns for large division. (B) The measured ringing voltage (bottom trace, vertical sensitivity 20 mV/div) of the TX loop–gap resonator after the application of the main pulse only (width of 350 ns). The arrow corresponds to the end of the main pulse. The time scale was 50 ns for large division and the measured dead time was 4000 ns. (C) The measured ringing voltage (bottom trace, vertical sensitivity 20 mV/div) of the TX loop–gap resonator after the application of the main pulse (width of 350 ns) and the auxiliary pulse (100 ns). The left arrow corresponds to the end of the main pulse and the right arrow corresponds to the start of the auxiliary pulse. The time scale was 50 ns for large division, and the measured dead time was 510 ns.

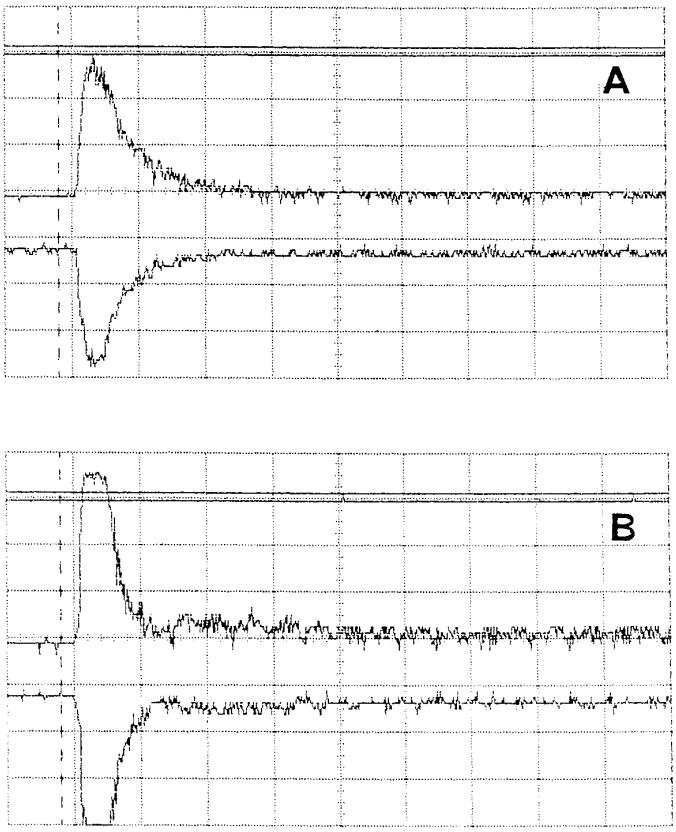

FIG. 6. (A) The measured ringing voltage with the single-channel detection (vertical sensitivity 1.5 V/div) using RX_S only (or RX_R only). The dotted vertical line corresponds to the end of the TX composite pulse (see Fig. 5A). The time scale was 100 ns for division and the measured dead time was about 450 ns. (B) The measured ringing voltage with the double-channel detection (vertical sensitivity 0.5 V/div) using RX_S and RX_R in the out-of-phase configuration. The dashed vertical line corresponds to the end of the TX composite pulse (see Fig. 5A). The time scale was 100 ns for division and the measured dead time was 300 ns.

220-MHz pulse was applied to the TX LGR, see Fig 5A. The duration of the TX pulse was 350 ns. To reduce the dead time of the TX resonator a further pulse, 100 ns in duration and 180° with respect to the first, was applied to the TX resonator (*30, 41*) (see Fig. 5A). With this quenching technique, we were able to minimize the T_D of the TX resonator, as reported in Figs. 5B and 5C. Because of the finite isolation, a fraction of the TX power leaks to the RX resonator, producing an additional ringing voltage. This ringing of the RX coils was measured with single-channel detection using RX_S only (or RX_R only), as reported in Fig. 6A, and with double-channel out-of-phase combination using RX_S and RX_R, see Fig. 6B. We observed that under this last condition T_D was less than 300 ns, giving rise to a reduction by about a factor of 10 with respect to the single-channel detection mode. The definition of dead time T_D requires some caution. The amplification chain of the spectrometer has a gain that makes it possible to bring the minimum detectable signal (that in theory is equal to the thermal noise voltage present in the observed bandwidth) to the level of the voltage step of the ADC. Ideally, once this gain is fixed the dead time of the instrument is the time required to reduce the amplified ringing voltage to that value.

With the current spectrometer design the TX channel can safely handle 80 W of power and the receive channel 800 W (with an isolation of 22 dB between the TX LGR and each RX resonator). The diodes used for protection (BAW62) can each sustain a peak current pulse of 0.45 A (with a duty factor of less then 0.35 and a pulse width of less then 0.5 ms), giving a power rating of 5W at 50 Ω. For the TX section 24 diodes are used in total, arranged in three sections of 8 diodes (4 forward, 4 backward); the peak current is thus 1.8 A, giving a pulse power rating of 80 W at 50 Ω. The 5 W of protection at the preamplifier inputs (MAN1-HLN) allows, with 22 dB of isolation, a possible TX power of 800 W. Thus no problem is anticipated for 90° pulses of 100 ns which require a TX power of about 50 W. At the output of the power combiner (using the out-of-phase configuration) the isolation increases to at least 45 dB. This, when added to the switch isolation (50 dB), more then protects the receiver from saturation at high power levels.

CW and FT EPR Detection

We used the CW EPR apparatus (Fig. 3) to demonstrate the EPR signal equivalence of the RX_S and RX_R receiving channels. A small sample (1.4 g) of DPPH (α,α'-diphenyl-β-picrylhydrazyl) was positioned at the center of the LGR, and the spectra were acquired under the following conditions: center field 8 mT, field span 1.5 mT, sweep time 50 s, time constant 300 ms. As shown in Fig. 7, the two spectra show a mixture of absorption and dispersion components. However, their signal amplitudes were similar, demonstrating experimentally the equivalence of the two receiving channels.

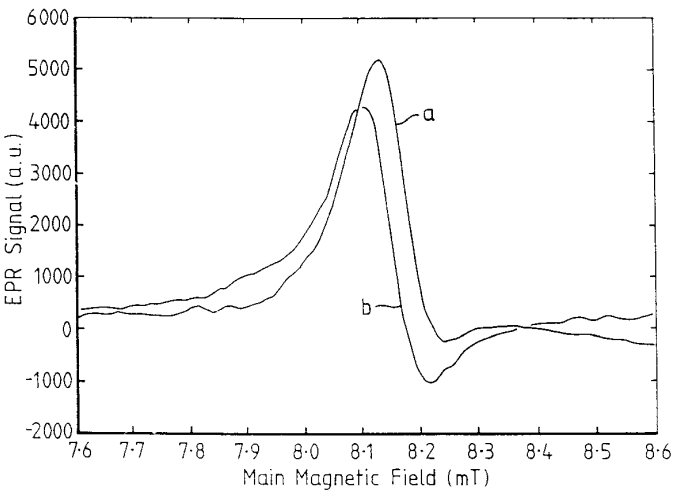

FIG. 7. CW EPR spectra of a DPPH sample obtained with the RX_S resonator only (a) or the RX_R resonator only (b). The spectra are a mixture of absorption and dispersion EPR components because no AFC was used.

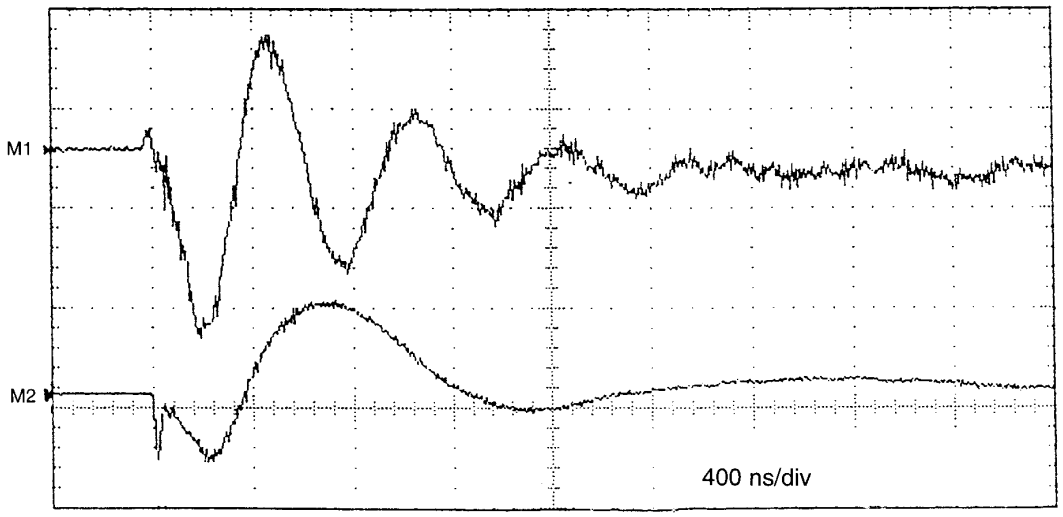

FIG. 8. EPR free induction decay (FID) signal obtained at 220.00 MHz with deoxygenated lithium phthalocyanine powder (1.5 g). The main field was 8.18 mT (top trace, vertical sensitivity 10 mV/div) and 8.14 mT (bottom trace, vertical sensitivity 40 mV/div). Each spectrum is the average of 10,000 FIDs obtained in 50 s.

Another very useful function of the CW EPR configuration is searching for the resonance when very-narrow-line (less than 300 mG) paramagnetic probes are used. A sample of 1.5 g of deoxygenated lithium phthalocyanine (LiPtc) powder contained in a small cylinder was inserted into a sample tube containing 50 ml of physiological solution (0.9% weight/volume of NaCl in deionized water). This sample was positioned in the center of the LGR and EPR spectra acquired under the following conditions: RF power 400 mW, center field 8.12 mT, field span 0.2 mT, sweep time 200 s, time constant 1 s. The approximate value of the filling factor (η) in this experiment was $\eta \approx 0.005$, obtained in a very crude approximation as $V_{\mathrm{SAMPLE}}/V_{\mathrm{RESONATOR}}$, in which $V_{\mathrm{RESONATOR}}$ is twice the internal resonator volume. We were unable to determine the exact value of η, as defined in Ref. (*39*) because we do not know the field distribution with enough accuracy. From the CW EPR spectra (results not shown) we calculated (*42*) an SNR of about 30. The measured linewidth was about 0.02 mT, and this value is consistent with previous work at L-band (1.2 GHz) (*43*). Because the CW EPR configuration was not optimized, the measured spectra give only a qualitative indication on the SNR. However, they provide a good indication of the signal level that should be expected with pulsed experiments.

For FT EPR spectroscopy 1.5 g of deoxygenated LiPtc powder sealed in a small cylinder (0.5 ml) was inserted into a sample tube containing 50 ml of physiological saline solution. The LiPtc was carefully positioned at the center of the LGR and under this condition the *Q* of the RX resonator was about 35. The duration of each 90° pulse was 360 ns and the repetition rate of the pulses was about 200 Hz. This long time was required by the refreshing rate of the oscilloscope. The digital oscilloscope was used in the average mode to acquire 10^4 FIDs in 50 s (see Fig. 8). A maximum SNR of about 20 was measured. The spin–spin relaxation T_2^* was estimated from the logarithm of the FID peak amplitude. A least-squares method to fit the data to a straight line with correlation coefficient better than 0.989 was used. For the deoxygenated LiPtc powder sample we obtained $T_2^* = (930 \pm 60)$ ns.

Some factors concerning the SNR of this configuration needs to be considered. The first is that there is not phase correlation between the noise generated by the two RX resonators. This means that theoretically the use of the double RX resonator increases the noise of the receiver by 3 dB. However, the dead time of the spectrometer is reduced, and the signal amplitude increases by a factor that depends on the particular experimental conditions. Of a different nature is the effect of the ''noise'' due to animal movement. Because of the geometry of the RX resonators the periodical variations of the RF parameters (resonant frequency, quality factor, and coupling coefficient) induced by animal motion in the two RX resonators are in-phase. Thus with the use of the double-channel receiver with out-of-phase combination (see Fig. 1), we do expect a minimal effect due to animal movements. However, we have not yet attempted *in vivo* experiments, and no experimental data are available.

CONCLUSIONS

We have presented an FT EPR instrument operating at 220 MHz that is suitable for large samples (up to 50 ml), uses separate high isolation (30 dB) TX and RX resonators, implements a composite TX pulse for the minimization of the TX ringing time, and uses two saddle-shaped resonators and a two-channnel receiver that greatly reduces the dead time (less than 300 ns). Examples of FID obtained with a deoxygenated LiPtc powder (1.5 g) showed a maximum

SNR of about 20 even with a low quality factor ($Q = 35$) RX resonator. We have shown that this instrument can be easly adapted for the CW detection of EPR spectra. The speed limit of the FT EPR apparatus is caused by the low repetition rate (200 Hz) of the digital oscilloscope used for data acquisition and display. However, fast digitizer/averager systems have been reported (*44, 45*), and we are currently developing a fast data acquisition circuit with a repetition rate of 200 kHz. This will allow our spectrometer to acquire 10^4 FIDs in 50 ms, giving rise to a decrease in the acquisition time of a factor of 1000, with respect to the CW EPR detection. Work is in progress to acquire EPR images using stationary field gradients and filtered back-projection techniques. The sample size and the gradient intensity determine the requirements for the bandwidth of the TX and RX resonators. For example, with a sample of 3 cm and a gradient intensity of 10 mT/m the required resonators bandwidth is 8.4 MHz. The TX and RX resonators presented in this work can fulfill this bandwidth requirement. The spatial resolution is determined by the linewidth of the paramagnetic probe and the gradient intensity (*1*). In previous *in vivo* CW EPR imaging studies with nitroxide free radicals (typical linewidth of 150 μT and gradient of 12 mT/m) the measured spatial resolution was 8 mm (*16*). Recently a single-line spin label with a linewidth of 6 μT suitable for *in vivo* applications has been reported (*46, 47*). The use of this spin label and gradient of 10 mT/m should produce a theoretical spatial resolution of 0.6 mm. The FT EPR apparatus was developed for very fast (less than 1min) detection and imaging of free radicals in biological systems such as whole rats and mice.

ACKNOWLEDGMENT

This work was supported in part by the Istituto Nazionale Fisica della Materia (INFM).

REFERENCES

1. K. Ohno, G. R. Eaton, and S. S. Eaton (Eds.), ''EPR Imaging and in vivo EPR,'' CRC Press, Boca Raton, FL (1991).
2. J. M. S. Hutchinson and J. Mallard, *J. Phys. E: Sci. Instrum.* **4,** 239 (1971).
3. M. Decorps and C. Fric, *J. Phys. E: Sci. Instrum.* **5,** 337 (1972).
4. H. J. Halpern, D. P. Spencer, J. van Polen, M. K. Bowman, A. C. Nelson, E. M. Dowey, and B. A. Teicher, *Rev. Sci. Instrum.* **60,** 1040 (1989).
5. J. Brivati, A. D. Stevens, and M. C. R. Symons, *J. Magn. Reson.* **92,** 480 (1991).
6. J. P. Hornack, M. Spacher, and R. G. Bryant, *Meas. Sci. Technol.* **2,** 520 (1991).
7. M. Alecci, S. Della Penna, A. Sotgiu, L. Testa, and I. Vannucci, *Rev. Sci. Instrum.* **63,** 4263 (1992).
8. H. Matsui, E. Yamada, S. Shimokava, and Y. Nakamura, *J. Phys. Chem.* **97,** 4284 (1993).
9. D. G. Gillies, L. H. Sutcliffe, and Mark R. Simms, *J. Chem. Soc. Faraday Trans.* **90,** 2671 (1994).
10. S. J. McCallum, M. Alecci, and D. J. Lurie, *Meas. Sci. Technol.* **7,** 1012 (1996).
11. K. Oikawa, T. Ogata, Y. Lin, T. Sato, R. Kudo, and H. Kamada, *Anal. Sci.* **11,** 885 (1995).
12. D. C. H. McBrien, and T. F. Slater, ''Free radicals, Lipid Peroxidation and Cancer,'' Academic Press, London (1982).
13. V. Quaresima, M. Alecci, M. Ferrari, and A. Sotgiu, *Biochem. Biophys. Res. Commun.* **183,** 829 (1992).
14. H. Ishida, S. Matsumoto, H. Yokoyama, N. Mori, H. Kumashiro, N. Tsuchihashi, T. Ogata, M. Yamada, M. Ono, T. Kitajima, H. Kamada, and E. Yoshida, *Magn. Reson. Imag.* **10,** 109 (1992).
15. H. J. Halpern, S. Pou, M. Peric, C. Yu, E. D. Barth, and G. R. Rosen, *J. Am. Chem. Soc.* **115,** 218 (1993).
16. M. Alecci, M. Ferrari, V. Quaresima, A. Sotgiu, and C. L. Ursini, *Bioph. J.* **67,** 1274 (1994).
17. M. Alecci, S. J. McCallum, M. A. Foster, D. J. Lurie, and I. Seimenis, *in* Proc. Society of Magnetic Resonance, Third Scientific Meeting, Nice, France, August 19–25 (1995).
18. S. J. McCallum, M. Alecci, and D. J. Lurie, *in* Proc. Society of Magnetic Resonance, Third Scientific Meeting, Nice, France, August 19–25 (1995).
19. T. Yoshimura, S. Fujii, H. Yokoyama, and H. Kamada, *Chem. Lett.* 309 (1995).
20. H. J. Halpern, M. Peric, C. Yu, E. D. Barth, G. V. R. Chamdramouli, M. W. Makinen, and G. R. Rosen, *Bioph. J.* **71,** 403 (1996).
21. T. Yoshimura, H. Yokoyama, S. Fujii, F. Takayama, K. Oikawa, and H. Kamada, *Nature Biotechnol.* **14,** 992 (1996).
22. G. Placidi, M. Alecci, and A. Sotgiu, *Rev. Sci. Instrum.* **65,** 58 (1994).
23. G. Placidi, M. Alecci, and A. Sotgiu, *J. Magn. Res. B* **108,** 50 (1995).
24. C. P. Poole and H. A. Farrach (Eds.), ''Handbook of Electron Spin Resonance. Data Sources, Computer Technology, Relaxation, and ENDOR,'' AIP Press, New York (1984).
25. R. J. Blume, *Phys. Rev.* **109,** 1867 (1958).
26. G. Sachs, W. Stocklein, B. Bail, E. Dormann, and M. Schwoerer, *Chem. Phys. Lett.* **89,** 179 (1982).
27. J. Bourg, M. C. Krishna, J. B. Mitchell, R. G. Tshudin, T. J. Pohida, W. S. Friauf, P. D. Smith, J. Metcalfe, F. Harrington, and S. Subramanian, *J. Magn. Reson. B* **102,** 112 (1993).
28. A. Coy, N. Kaplan, and P. T. Callaghan, *J. Magn. Reson. A* **121,** 201 (1996).
29. E. Fukushima and S. B. W. Roeder, ''Experimental Pulse NMR. A Nuts and Bolts Approach,'' p. 309, Addison-Welsey, London (1981).
30. P. A. Narayana, R. J. Massoth, and L. Kevan, *Rev. Sci. Instrum.* **53,** 624 (1982).
31. C. N. Chen and D. I. Hoult, ''Biomedical Magnetic Resonance Technology,'' IOP, Bristol, UK (1989).
32. J. A. Pople, W. G. Scheider, and H. J. Bernstein, ''High-Resolution NMR,'' McGraw–Hill, New York (1959).
33. D. J. Lurie, S. J. McCallum, J. M. S. Hutchison, and M. Alecci, *MAGMA* **4,** 77 (1996).
34. G. A. Rinard, R. W. Quine, and G. R. Eaton, *in* Proc. 19th Int. EPR Symposium, 38th Rocky Mountain Conference on Analytical Chemistry, Abstract 147, Denver, July 21–26 (1996).
35. C. P. Keijers, E. J. Reijerse, and J. Schmidt (Eds), ''*Pulsed EPR: A New Field of Applications,*'' p. 47, North Holland, Amsterdam (1989).
36. W. Froncisz and J. S. Hyde, *J. Magn. Reson.* **47,** 515 (1982).

37. E. L. Gintzon, ''Microwave Measurements,'' McGraw–Hill, New York (1957).

38. M. Alecci, J. A. Brivati, G. Placidi, L. Testa, D. J. Lurie, and A. Sotgiu, submitted (1997).

39. C. P. Poole, ''Electron Spin Resonance,'' p. 394, Interscience, New York (1967).

40. M. Alecci, S. J. McCallum, and D. J. Lurie, *J. Magn. Reson. A* **117,** 272 (1995).

41. J. L. Davis and W. B. Mims, *Rev. Sci. Instrum.* **52,** 131, (1981).

42. R. R. Ernst, *Adv. Magn. Reson.* **2,** 1 (1966).

43. K. J. Liu, P. Gast, M. Moussavi, S. W. Norby, N. Vahidi, T. Walczak, M. Wu, and H. M. Swartz, *Proc. Natl. Acad. Sci. USA* **90,** 5438 (1993).

44. R. Ambrosetti and D. Ricci, *Rev. Sci. Instrum.* **62,** 2281 (1991).

45. T. J. Pohida, H. A Fredrickson, R. G. Tschudin, J. F. Fessler, M. C. Krishna, J. Bourg, F. Harrington, and S. Subramanian, *Rev. Sci. Instrum.* **65,** 2500 (1994).

46. P. Kuppusamy, P. Wang, M. Chzhan, and J. L. Zweier, Abstracts of the International Society of Magnetic Resonance in Medicine, Vancouver, p. 2130, (1997).

47. H. Konijnenburg, J. Trommel, J. H. Ardenkjaer-Larsen, and A. F. Mehlkopf, Abstracts of the International Society of Magnetic Resonance in Medicine, Vancouver, p. 2129, (1997).